Sedimentary Geology 363 (2018) 83–95

Contents lists available at ScienceDirect

Sedimentary Geology

journal homepage: www.elsevier.com/locate/sedgeo

Late Cretaceous paleosols as paleoclimate proxies of high-latitude Southern Hemisphere: Mata Amarilla Formation, Patagonia, Argentina

Augusto N. Varela [a,b,*], M. Sol Raigemborn [a,b], Sebastián Richiano [c], Tim White [d], Daniel G. Poiré [a,e], Sabrina Lizzoli [f]

[a] CONICET – UNLP, Centro de Investigaciones Geológicas, Diagonal 113 275, B1904DPK La Plata, Argentina
[b] Cátedra de Micromorfología de Suelos, Facultad de Ciencias Naturales y Museo, Calle 122 y 60 s/n, 1900 La Plata, Argentina
[c] CONICET – CENPAT, Instituto Patagónico de Geología y Paleontología, Boulevard Brown 2915, 9120 Puerto Madryn, Chubut, Argentina
[d] Earth and Environmental Systems Institute, The Pennsylvania State University, University Park, PA 16802, United States
[e] Cátedra de Rocas Sedimentarias, Facultad de Ciencias Naturales y Museo, Calle 122 y 60 s/n, 1900 La Plata, Argentina
[f] UNLP, Cátedra de Geología Estructural, Facultad de Ciencias Naturales y Museo, Calle 122 y 60 s/n, 1900, La Plata, Argentina

ARTICLE INFO

Article history:
Received 22 August 2017
Received in revised form 2 November 2017
Accepted 3 November 2017
Available online 08 November 2017

Editor: Dr. J. Knight

Keywords:
Paleoclimatology
Pedogenesis
Climofuntions
Pedogenic processes
Austral/Magallanes Basin
Cenomanian–Santonian

ABSTRACT

Although there is general consensus that a global greenhouse climate characterized the mid-Cretaceous, details of the climate state of the mid-Cretaceous Southern Hemisphere are less clearly understood. In particular, continental paleoclimate reconstructions are scarce and exclusively derived from paleontological records. Using paleosol-derived climofunction studies of the mid- to Upper Cretaceous Mata Amarilla Formation, southern Patagonia, Argentina, we present a reconstruction of the mid-Cretaceous climate of southern South America. Our results indicate that at ~60° south paleolatitude during the Cenomanian–Santonian stages, the climate was subtropical temperate–warm (12 °C ± 2.1 °C) and humid (1404 ± 108 mm/yr) with marked rainfall seasonality. These results are consistent with both previous estimations from the fossil floras of the Mata Amarilla Formation and other units of the Southern Hemisphere, and with the previous observations of the displacement of tropical and subtropical floras towards the poles in both hemispheres. The data presented here show a more marked seasonality and slightly lower mean annual precipitation and mean annual temperature values than those recorded at the same paleolatitudes in the Northern Hemisphere.

1. Introduction

Paleosols can be useful and direct paleoclimatic proxies due to the fact that soil forms at Earth's surface, recording the atmospheric and climatic conditions during formation (e.g., Lal, 1999, 2004; Retallack, 2001; White et al., 2001; Sheldon et al., 2002; Nordt and Dreise, 2010). In particular, soil clay minerals can be correlated with climate factors such as temperature and water availability due to the fact that these factors strongly affect chemical weathering in the soil profile (see review in Sheldon and Tabor, 2009). In addition, there are key elemental ratios (Sheldon and Tabor, 2009) and weathering indices (Maynard, 1992; Sheldon et al., 2002; Nordt and Dreise, 2010) that serve as proxies for different pedogenic processes and for determining the weathering intensity in paleosols. Further, paleosol geochemistry can allow for the determination of quantitative climate parameters such as paleotemperature and paleoprecipitation (e.g., Sheldon and Tabor, 2009; Adams et al., 2011; Hyland et al., 2015, among others).

Mid-Cretaceous climate reconstructions indicate that greenhouse conditions prevailed, with a globally averaged mean annual temperature (MAT) of ~8 °C greater than present (Barron, 1983; Caldeira and Rampino, 1991; Frakes, 1999; Poulsen et al., 1999, 2001, 2007; Royer, 2010; Hay, 2011). The present pole-to-equator sea-level temperature difference is ~50 °C, whereas that of the mid-Cretaceous ranged from 30 °C to as little as 24 °C, implying a warm and more uniform climate (Barron, 1983; Frakes, 1999; Poulsen et al., 1999, 2001, 2007; Hay, 2011). The increased poleward heat transfer by H_2O vapor may explain these reduced equator-to-pole temperature gradients (Ufnar et al., 2004; Hay, 2011). Likewise, an atmospheric pCO_2 four times higher than present values may have increased average annual precipitation (MAP) globally by 25% (Barron et al., 1989; White et al., 2001, 2005; Royer, 2010; Ludvigson et al., 2015). Paleosol data from the North American Cretaceous Western Interior Basin and mass-balance modeling suggest that mid-Cretaceous precipitation rates exceeded modern rates at both mid- and high-latitudes; and also suggest amplification of the mid-Cretaceous atmospheric hydrologic cycle (White et al., 2001; Ufnar et al., 2004; Poulsen et al., 2007).

All global models of continental precipitation and climatic conditions of the mid-Cretaceous are based on paleofloral assemblages

* Corresponding author at: CONICET – UNLP, Centro de Investigaciones Geológicas, Diagonal 113 275, B1904DPK La Plata, Argentina.
E-mail address: augustovarela@cig.museo.unlp.edu.ar (A.N. Varela).

https://doi.org/10.1016/j.sedgeo.2017.11.001
0037-0738/

and paleosol data from the Northern Hemisphere, and are especially concentrated in the Western Interior Basin of the U.S.A. (e.g., Barron et al., 1989; Poulsen et al., 1999, 2001, 2007; White et al., 2001, 2005; Ufnar et al., 2002, 2004; Floegel and Wagner, 2006). In the Southern Hemisphere, all mid-Cretaceous reconstructions are based on fossil evidence, e.g., angiosperm and conifer floras, and palynology (Parrish et al., 1998; Iglesias et al., 2007; Pole and Philippe, 2010; Cantrill and Poole, 2012; Fletcher et al., 2014; Bowman, 2015).

Here we expand the evidence from South America by incorporating reconstructions based on paleosol data from Argentina. The focus is on the Mata Amarilla Formation in southern Patagonia, Argentina, because it contains a complete mid-Cretaceous high-latitude succession of paleosols. This succession provides an excellent opportunity to: i) characterize the main pedogenic processes using micromorphological and clay mineralogical analyses, and paleosol geochemistry; ii) constrain the paleoclimatic conditions, e.g., MAP and MAT, and seasonality; and, iii) make the first interhemispheric comparison of the mid-Cretaceous global climate based on paleosol data.

2. Geological background

The Mata Amarilla Formation (mid-Cretaceous) is a terrestrial succession in southern Argentinean Patagonia related to the foreland stage of the Austral/Magallanes Basin (Varela, 2015) (Fig. 1a). Through a sedimentological and sequence stratigraphic analysis, Varela (2015) divided the Mata Amarilla Formation into three informal sections (lower, middle and upper; Fig. 1b). The contact between the underlying Piedra Clavada Formation and the lower section of Mata Amarilla Formation has been assigned to the Albian-Cenomanian boundary (~100 Ma; Varela et al., 2012a), based on the occurrence of *Monhria* spores (Archangelsky, 2009). Recent radiometric dates from the uppermost Piedra Clavada Formation confirm this age (101 ± 0.9 Ma and 99 ± 2.8 Ma; Poiré et al., 2017). The middle section has been dated at 96.23 ± 0.71 Ma (middle Cenomanian; Varela et al., 2012a). The contact with the overlying La Anita Formation (Campanian) is erosive (Fig. 1b). The study area is located in the southwest of Santa Cruz Province, Argentina (southern Patagonia, Fig. 1a). The results of previous detailed sedimentological and paleopedological studies (Varela et al., 2012b, 2016; Varela, 2015) led to the selection of the Cerro Waring locality because it has the most complete stacked paleosol succession (130 m thick) of this unit (Fig. 1b).

The Mata Amarilla Formation is composed of grey and black mudstones, alternating with 1–10 m-thick white fine- to medium-grained sandstones, deposited in continental and littoral environments (Varela et al., 2011; Varela, 2015). The lower section of Mata Amarilla Formation is characterized by distal fluvial, coastal plain and littoral marine facies developed in a large embayment. The middle section is characterized by a lowstand wedge constituted from west to east by strata deposited in braided, high-sinuosity meandering and low-sinuosity meandering fluvial environments. Finally, the upper section of Mata Amarilla Formation is also characterized by a distal fluvial and coastal plain facies developed in a large embayment (Varela et al., 2011; Varela, 2015). The unit was located at high mid-paleolatitudes during deposition (58.11° south latitude; according to Van Hinsbergen et al., 2015) and records a distinctive suite of paleosols with Vertisols as the most abundant, and Inceptisols, Histosols and vertic Alfisols present in minor proportions (Varela et al., 2012b).

Histosols were developed in topographically low coastal areas, with very poor drainage conditions (wetlands) in the lower and upper sections of the formation. Vertisols and Inceptisols are present throughout the succession in a catenary relationship within the fluvial systems (Inceptisols were developed in levees and crevasse deposits while Vertisols developed in floodplains). Finally, vertic Alfisols are restricted to the sequence boundary between the lower and middle section of the Mata Amarilla Formation (Varela et al., 2012b, 2016).

3. Methodology

Paleosols were identified in outcrop based on macroscopic pedofeatures such as structure, mottles, nodules, color, slickensides, cutans and rhizoliths (e.g., Retallack, 2001). Paleosol horizons, thickness, contact types, mean grain size, ped structure, type of nodules and evidence of bioturbation were described (e.g., Soil Survey Staff, 1975, 1998; Retallack, 2001). The paleosols (lithified material) were trenched to a depth of >30 cm to avoid modern contamination (Fig. 2a). Twenty-three samples for paleosol thin-sections were obtained for micromorphological analysis. Mean grain size, mineralogical composition, porosity, microstructure, microfabrics, groundmass and pedofeatures were studied following the criteria of Bullock et al. (1985) and Stoops (2003), in order to characterize the kind and intensity of various paleopedogenic processes. Also, a systematic sampling was performed from all identified paleosol horizons for X-ray diffraction (XRD) clay mineralogical analysis (n = 103; Supplementary Table 1). Diffractograms were run on a PANalytical X'Pert PRO diffractometer (Centro de Investigaciones Geológicas, La Plata, Argentina), using Cu radiation (Kα = 1.5405 Å) and Ni filter and generation settings of 40 kV and 40 mA. Routine air-dried mounts were run between 2 and 32° 2θ at a scan speed of 2° 2θ/min. Ethylene glycol-solvated and heated samples were run from 2 to 27° 2θ and 3 to 15° 2θ, respectively, at a scan speed of 2° 2θ min. Semi-quantitative estimations of the relative

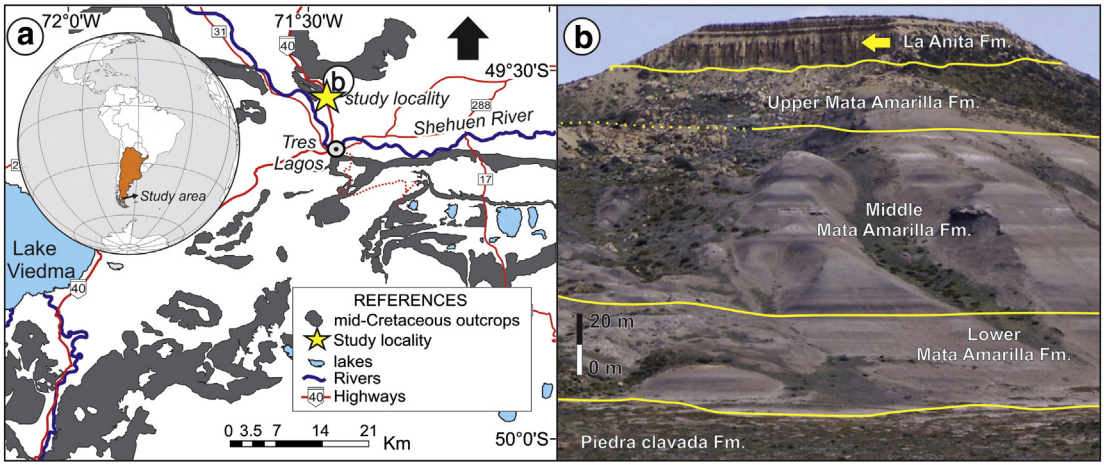

Fig. 1. (a) Geological setting and location of the study area showing the mid-Cretaceous outcrops. (b) Panoramic photograph of the Mata Amarilla Formation at Cerro Waring locality where stacked mid-Cretaceous paleosols occur.

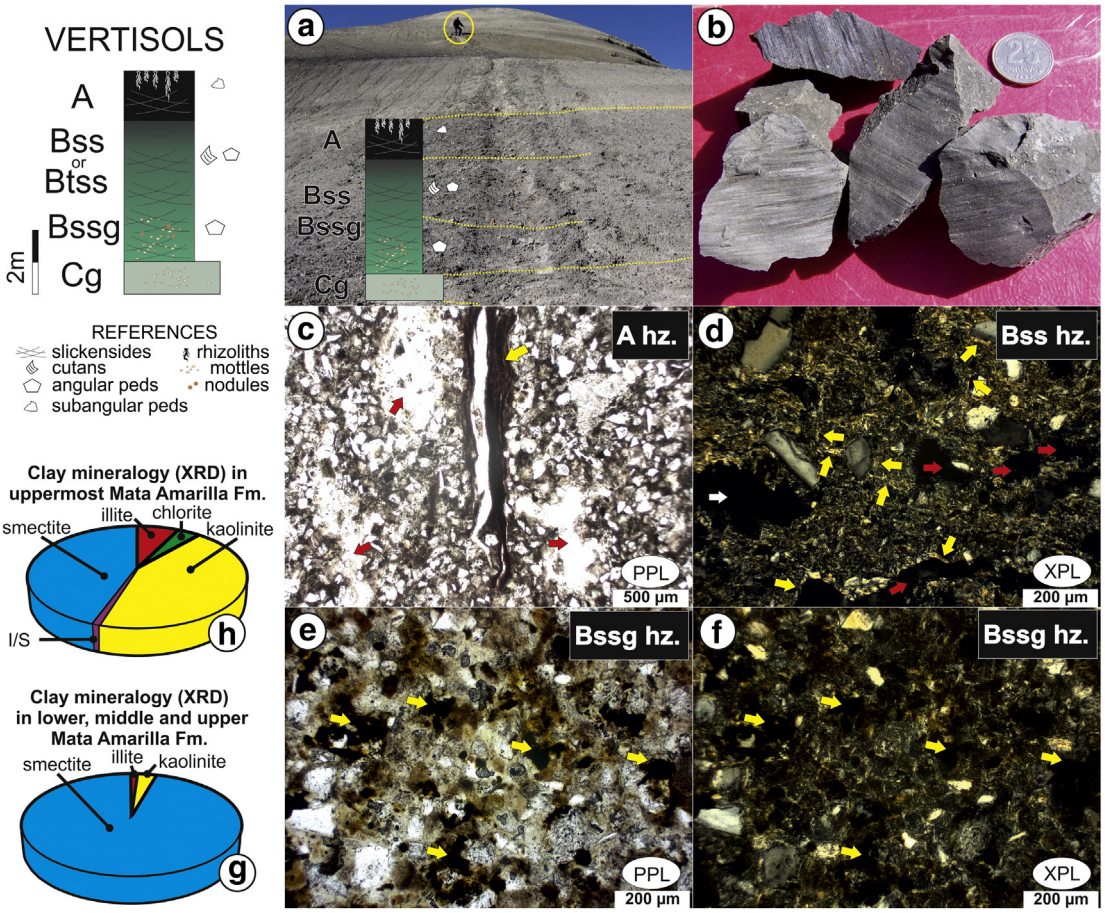

Fig. 2. Vertisol features (a) Field picture of a Vertisols succession showing the trench, person for scale is 1.75 m. (b) Detail of angular wedge-shaped peds with slickensides, coin for scale is 2.2 cm. Detailed micromorphology of (c) A horizon showing dark color groundmass, compound-packing voids, chambers (red arrows), and a rhizolith with a thick laminated clay coating their walls (yellow arrow), Plane Polarized Light (PPL). (d) Bss horizon showing double space to open porphyric c/f related distribution, light brown groundmass with cross-striated b-fabric characterized by two set of birefringent clay orientation ~80° (yellow arrows), channels (red arrows) and chamber (white arrow). Cross Polarized light (XPL). (e) Bssg horizon showing typic Fe-Mn nodules moderately to strongly impregnate with amiboidal and aggregated morphologies (yellow arrows), PPL. (f) Fe-Mn nodules partially obliterating cross-striated b-fabric (yellow arrows), XLP. (f) Clay mineralogical composition of Vertisols from lower middle and upper Mata Amarilla Fm. (g) Clay mineralogical composition of Vertisols from the uppermost Mata Amarilla Fm. (For interpretation of the references to colour in this figure legend, the reader is referred to the web version of this article.)

percentages of clay minerals were based on the peak area method (Biscaye, 1965) on glycolated samples (001 for illite, smectite, kaolinite, palygorskite and illite/smectite mixed layer; chlorite/smectite, kaolinite/smectite, and 002 for chlorite) by applying empirical factors (Moore and Reynolds, 1989).

A detailed sampling strategy of B horizons for geochemical analyses was performed following the criteria of Hyland and Sheldon (2016), noting that there is no evidence that diagenesis has modified the geochemistry of the sediment and paleosols. Major element composition methodology involved the whole-rock analyses of B horizon samples using Inductively Coupled Plasma Atomic Emission Spectrometry (ICP-AES) at The Pennsylvania State University, USA. Samples were fused using lithium metaborate and run on a Perkin-Elmer Optima 5300 (ICP-AES), where the analytical uncertainty is at <0.1% and mean standard deviation was 0.09%. Data from major oxide analyses were converted from weight percent to molar percent to calculate paleosol indices and paleoclimate proxies discussed below. The pedogenic process indices used were: for weathering processes, CIA-K, where CIA-K = 100 × [(Al/(Al + Ca + Na)] (Maynard, 1992), and CALMAG, where CALMAG = 100 × [(Al/(Al + Ca + Mg)] (Nordt and Dreise, 2010); for hydrolysis of alkaline earth elements, loss of exchangeable bases, Al/∑Bases ratio (Retallack, 2001); for clayeyness, Al/Si ratio (Sheldon and Tabor, 2009); for oxidation total iron/alumina ratio (Retallack, 2001); for salinization SAL = (Na + K)/Al (Retallack, 2001); and for changes in paleosol provenance, Ti/Al ratio (Sheldon, 2006).

Mean annual temperature (MAT) proxies were calculated based on the SAL ratio from Sheldon et al. (2002) and PWI (Paleosol Weathering Index) from Gallagher and Sheldon (2013). The mean annual temperature equation is MAT = −18,516 (SAL) + 17,298 (Sheldon et al., 2002). The error associated with this SAL-based MAT estimation is ±4.4 °C and can be applied to most paleosol orders (Sheldon et al., 2002). The PWI-based MAT equation of Gallagher and Sheldon (2013) is MAT = 2.74 ln (PWI) + 21.39, where PWI = 100 x [(4.20 × Na) + (1.66 x Mg) + (5.54 × K) + (2.05 × Ca)]. This MAT estimation is better constrained, and the standard error in MAT values associated with this equation is ±2.1 °C (Gallagher and Sheldon, 2013).

Mean annual precipitation (MAP) was calculated with different quantitative proxies. The first paleoprecipitation calculation was the MAP estimation based on ∑Bases/Al where MAP = −259.3 ln (∑Bases/Al) + 759, with a standard error of ±235 mm yr^{-1} (Sheldon et al., 2002). The second paleoprecipitation estimation was the MAP proxy based on the CIA-K index of Maynard (1992), where MAP = 221.12$e^{0.0197(CIA-K)}$ with a standard error ± 181 mm yr^{-1} (Sheldon et al., 2002). Finally, the last paleoprecipitation calculation was the MAP proxy developed specifically for Vertisols based on the CALMAG index, where MAP = 22.69 (CALMAG)–435.8, with a standard error ± 108 mm/yr (Nordt and Dreise, 2010). Comparative studies indicate that the CALMAG-based MAP estimation is more accurate than CIA-K-based MAP estimation for vertic paleosols (Nordt and Dreise, 2010; Adams et al., 2011).

Classification of the paleosols was made based on the field morphology, micromorphology and with the compositional analyses (XRD and geochemical data) following the criteria of USDA, Soil Taxonomy (1975, 1998) and the modifications for paleosols by Retallack (1993).

4. Results

4.1. The paleosols of the Mata Amarilla Formation

The Mata Amarilla paleosols are characterized macromorphologically by well-structured horizons, gley-colors, slickensides, angular blocky to wedge shaped peds, cutans, mottles and rhizoliths. These paleosols were classified following Soil Taxonomy (Soil Survey Staff, 1975, 1998; Retallack, 1993) as Vertisols (60%), Histosols (25%), Inceptisols (12%) and vertic Alfisols (3%), listed in order of abundance. The lower section comprised the development of Histosol and Vertisols in coastal plain environments. The middle section has a highly mature vertic Alfisol related to a forced regressive surface (Varela et al., 2016) and the remainder is constituted by Vertisols and Inceptisols in a catenary relationship within fluvial sub-environments. The upper section is composed of Histosols and Vertisols in coastal plain environments (Varela et al., 2012b).

4.2. Macro and micromorphological description

4.2.1. Vertisols

They are the most abundant paleosol in the Mata Amarilla Formation. They show thick well-developed horizons with greenish grey matrix with low chromas, and profiles with A-Bss (B horizon with slickensides), and sometimes Btss (B horizon with illuvial accumulation of clay and slickensides), -Bssg (B horizon with slickensides and gleying hydromorphic features), and -Cg (C horizon with gleying hydromorphic features) successions (Fig. 2a); in many cases, eroded tops with the absence of an A horizon were observed. The most typical morphological features are slickensides, angular peds (Fig. 2b), yellowish and greenish-grey rhizoliths (root casts, rhizotubules, rhizocretions and/or rhizohaloes), yellowish to brownish and bluish grey mottles and 0.5 and 20 mm yellowish to dark brown Fe-Mn nodules.

The coarse fraction of these Vertisols is composed of silt to very fine sand particles of quartz, feldspar and volcanic lithic grains. These lithic grains show felsitic, pilotaxic and trachytic textures (intermediate and acidic volcanic fragments), with a mostly high degree of alteration. When present, the A horizons show clay loam to very fine sand particle size classes and a coarse/fine ($c/f_{=3.9\ \mu m}$) ratio from 1/2 to 1/3. The c/f-related distribution is close porphyric. The groundmass shows dark color with an undifferentiated b-fabric; the absence of interference color in the groundmass is mask by organic matter and Fe-oxides. Compound-packing voids, chambers and less frequently channels are preserved in the groundmass (Fig. 2c). Rhizoliths are abundant and usually show thick laminated brown to dark brown dusty clay coatings covering their walls (Fig. 2c). Bss horizons show clay loam to silt to very fine sand particle size classes and a coarse/fine ($c/f_{=3.9\ \mu m}$) ratio from 1/3 to 1/4. The c/f-related distribution is double space to open porphyric (Fig. 2d). The groundmass shows light brown color with cross-striated b-fabric characterized by two sets of birefringent clay oriented at an angle of ~80°. Different kinds of voids, channels and chambers (Fig. 2d), with frequent thin non-laminated yellowish dusty clay coating around their walls are also present. When these illuvial features are more abundant, the B horizons are classified as Btss. Bssg horizons have the same micromorphological characteristics as the Bss horizons, except for the presence of abundant Fe-Mn nodules. These nodules are typically moderately to strongly impregnated with amiboidal and aggregated morphologies; the average sizes are between 50 and 250 μm (Fig. 2e, f). The clay mineralogy of these Vertisols is dominated by smectite (~96%) and a very minor proportion of kaolinite (~3%; Fig. 2g), except in the uppermost Mata Amarilla Formation where Vertisols reach up to ~40% of kaolinite (Fig. 2h).

4.2.2. Histosols

They are present in the lower and upper sections of the Mata Amarilla Formation. They show stacks of thin profiles with Oe (O horizon with organic matter intermediate in decomposition)-A-Bg (B horizon with gleying hydromorphic features) successions (Fig. 3). The most important macromorphological features are dark grey to black mottles of small carbonaceous remains disseminated in the paleosol matrix as well as orange and purplish-blue mottles (Fig. 3a). Slickensides and rhizoliths are also abundant; greenish-grey rhizoliths and fossil roots are mostly preserved as carbonaceous material (Fig. 3b). The coarse fraction of these paleosols consist of very fine to fine sand grains of quartz, feldspar and intermediate to acidic volcanic fragment (felsitic, pilotaxic and trachytic textures) showing different degrees of alteration. Oe horizons show clay loam to fine sand particle size classes and a coarse/fine ($c/f_{=3.9\ \mu m}$) ratio from 1/1 to 1/2 (Fig. 3c, d). The c/f-related distribution is enaulic to close porphyric (Fig. 3c). The coarse organic components are abundant and comprise mostly dark plant tissue residues with a high degree of preservation (cell structures are clearly recognizable) and less frequently highly decomposed dark plant organ residues (Fig. 3c, d). The groundmass shows dark brown to black color (by the presence of fine amorphous organic matter and Fe/Mn-oxides) with an undifferentiated b-fabric. Simple-packing voids, chambers and channels are preserved in the groundmass (Fig. 3c, d). Plant residues and fine amorphous organic matter is laminated between mineral-dominated layers. A horizons show clay loam to silt to very fine sand particle size classes and a coarse/fine ($c/f_{=3.9\ \mu m}$) ratio from 1/4 to 1/5. The c/f-related distribution is double space to open porphyric (Fig. 3e). Coarse organic components are rarely present, showing black color, undifferentiated morphology, and low degree of preservation (Fig. 3e). The groundmass shows fine amorphous organic matter, punctuations and organic pigment with dark brown to black color and undifferentiated b-fabric. Simple-packing voids are often preserved in the groundmass. Bg horizons show clay loam to very fine sand particle size classes and a coarse/fine ($c/f_{=3.9\ \mu m}$) ratio from 1/1 to 1/2. The c/f-related distribution is enaulic to close porphyric. Channels, chambers and simple-packing voids are preserved in the groundmass, which shows light to more dark brown color with an undifferentiated b-fabric (Fig. 3f). Fine amorphous organic matter is occasionally dispersed in the groundmass. As diagnostic pedofeatures, Bg horizons show abundant Fe-Mn nodules. These are typically strongly impregnated to pure with rounded morphologies, and less frequently amiboidal and aggregate morphologies; the average sizes are between 50 and 180 μm (Fig. 3f). Although the Histosols of Mata Amarilla Formation are macro and micro-morphologically very similar, the mineralogical composition of the clays change according to stratigraphic position in the unit; in the lower section they are composed of ~55% smectite and ~38% palygorskite with very scarce kaolinite at ~5% (Fig. 3g), while in the upper section they are dominated by ~67% smectite and ~33% kaolinite (Fig. 3h).

4.2.3. Inceptisols

Inceptisols and Vertisols are present in a catenary relationship within the fluvial channels, whereas Inceptisols were developed in levees and crevasse splay deposits (Varela et al., 2012b). Inceptisols display relatively thin moderately to poorly developed and stacked profiles with A-Bw or B/C-C successions (Fig. 4a). Inceptisols are characterized macroscopically by poorly developed horizonation where the most important features are yellowish to brownish rhizoliths, mottles and Fe-Mn nodules. The Bw and B/c horizons are generally non-structured massive with poor ped developments (Fig. 4b).

The coarse fraction is constituted of quartz, feldspar and fresh to low degree of alteration volcanic lithic fragments with felsitic, pilotaxic and trachytic textures. The A horizons show clay loam to very fine sand particle size classes. The mineral coarse fraction is composed of very fine sand grains and the coarse/fine ($c/f = 3.9\ \mu m$) ratio varies from 1/1 to 1/2 T. The c/f-related distribution is gefuric to chitonic (Fig. 4c). The groundmass is light to dark brown by the occurrence of organic matter

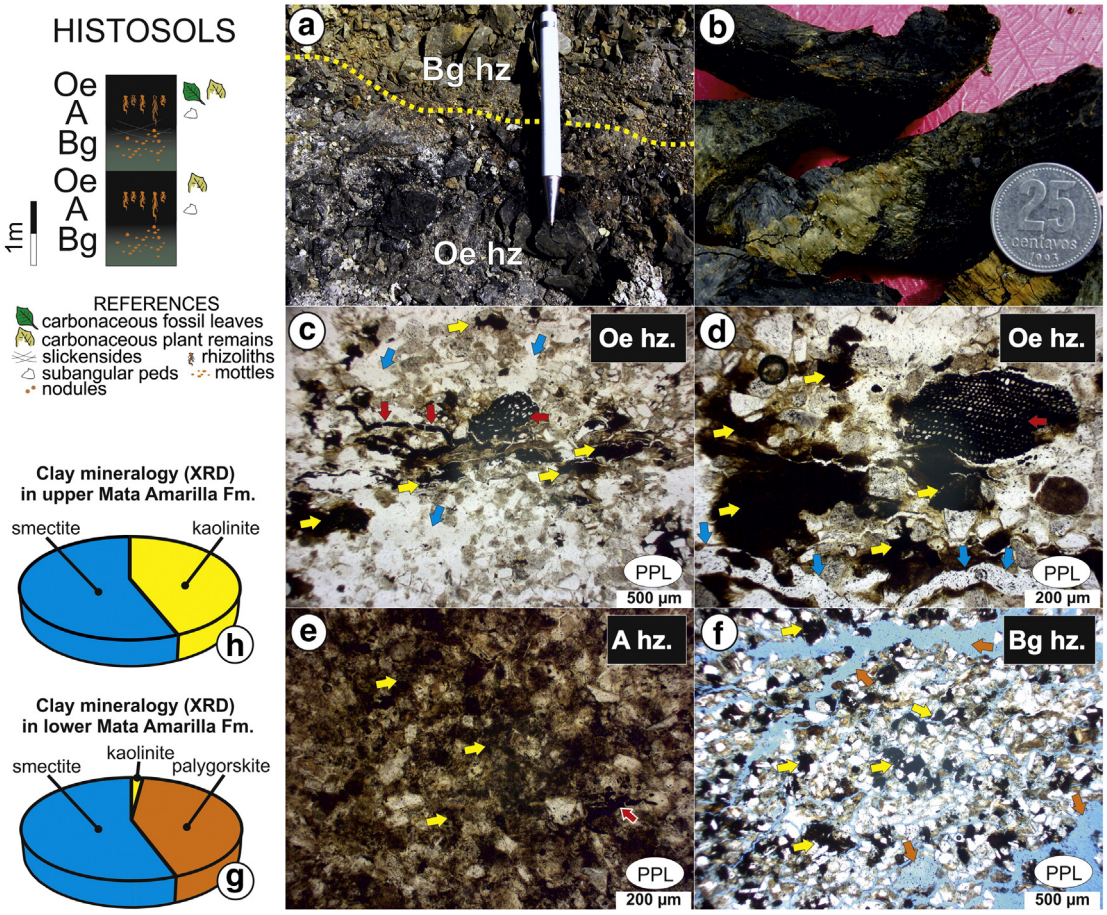

Fig. 3. Histosol features. (a) Field picture showing the dark colored Oe horizon, overlying by a gley colored Bg horizon, pen for scale is 14 cm. (b) Detail of dark colored subangular peds from A horizon, coin for scale is 2.2 cm. Detailed micromorphology of (c) Oe horizon showing well preserved plant tissues (red arrows), highly decomposed dark plant residues (yellow arrows), and chambers in the groundmass (blue arrows), PPL. (d) Detail of poorly decomposed plant tissue where cell structures are clearly recognizable (red arrow), decomposed dark brown to black plant residues (yellow arrows), and a large channel (blue arrows), PPL. (e) A horizon showing dark brown to black groundmass composed by amorphous organic matter fine material and organic pigment (yellow arrows), and a poorly preserved dark plant residues (red arrow), PPL. (f) Bg horizon showing typic strongly impregnate to pure Fe-Mn nodules with amiboidal and aggregate morphologies (yellow arrows), and channels and chambers (orange arrows), PPL. (g) Clay mineralogical composition of Histosols from lower Mata Amarilla Fm. (h) Clay mineralogical composition of Histosols from the upper Mata Amarilla Fm. (For interpretation of the references to colour in this figure legend, the reader is referred to the web version of this article.)

with an undifferentiated b-fabric. Simple-packing voids and chambers are preserved in the groundmass. As characteristic pedofeatures these Inceptisols show abundant typic Fe-Mn nodules strongly impregnated with amiboidal morphologies; the average sizes are between 40 and 200 µm (Fig. 4c). The Bw and B/C horizons show clay loam to very fine sand particle size classes, the coarse fraction is composed of fine to very fine sand particles and the coarse/fine (c/f $_{= 3.9\ \mu m}$) ratio ranges from 1/1 to 1/2 (Fig. 4d, e). The c/f-related distribution is chitonic to gefuric. The groundmass is light brown with an undifferentiated b-fabric (Fig. 4d, e). Simple-packing voids are preserved in the groundmass. These horizons show similar Fe-Mn nodules as in A horizons (Fig. 4d, e). The C horizons show medium to coarse sand particle size classes and a coarse/fine (c/f $_{= 3.9\ \mu m}$) ratio of 10/1. The c/f-related distribution is monic (Fig. 4f). The sand grains show thin non-laminated gray limpid clay coatings as the unique characteristic pedofeatures (Fig. 4f). The clay mineralogy of these Inceptisols is similar to vertisols only with a slightly higher percentage of kaolinite. Inceptisols are dominated by ~88% smectite with a scarce proportion of kaolinite ~12% (Fig. 4g).

4.2.4. Alfisols

They are present only in the level between the lower and middle section of the Mata Amarilla Formation and show thick well-developed profiles with A-A/E-Bt (B horizon with illuvial accumulation of clay) –Bss (B horizon with slickensides) succession (Fig. 5a). The most typical morphological features of these paleosols are: well-structured Bt horizon with prismatic peds and abundant cutans (Fig. 5b); as well as, slickensides, angular peds, mottles, and Fe-Mn nodules in the Bss horizon. The coarse fraction of these Alfisols is composed of silt to very fine sand particles of quartz, feldspar and volcanic lithic grains. These lithic grains present felsitic, pilotaxic and trachytic textures with high degree of weathering. The A horizons show similar micromorphological features as the A-horizons in Vertisols. This Alfisol presents a poorly defined A/E horizon with fine sand particle size classes and monic c/f related distribution as main features. The diagnostic Bt horizon shows clay loam to very fine sand particle size classes and a coarse/fine (c/f $_{= 3.9\ \mu m}$) ratio from 1/4 to 1/6 (Fig. 5c, d). The c/f-related distribution is chitonic to double-space porphyric (Fig. 5c, d). The groundmass is light to brown with an undifferentiated b-fabric. Only small voids related to some rhizolith walls are preserved in the groundmass (Fig. 5c). The diagnostic pedofeature is the presence of abundant laminated to microlaminated, dense, complete to incomplete yellowish brown dusty illuvial clay infillings (Fig. 5c, d). The Bss horizon shows clay loam to fine sand particle size classes and a coarse/fine (c/f $_{= 3.9\ \mu m}$) ratio from 1/2 to less frequently 1/3. The c/f-related distribution is chitonic to simple/double space porphyric. The groundmass is light brown to orange with cross-striated b-fabric; characterized by two sets of birefringent clay oriented at an angle of ~80° (Fig. 5e, f). The b-axes of grains are also oriented with the same pattern (Fig. 5f). The clay mineralogy of these vertic Alfisols is dominated by smectite (~95%) with minor proportions of kaolinite (~4%) and illite and chlorite (<1%) (Fig. 5g).

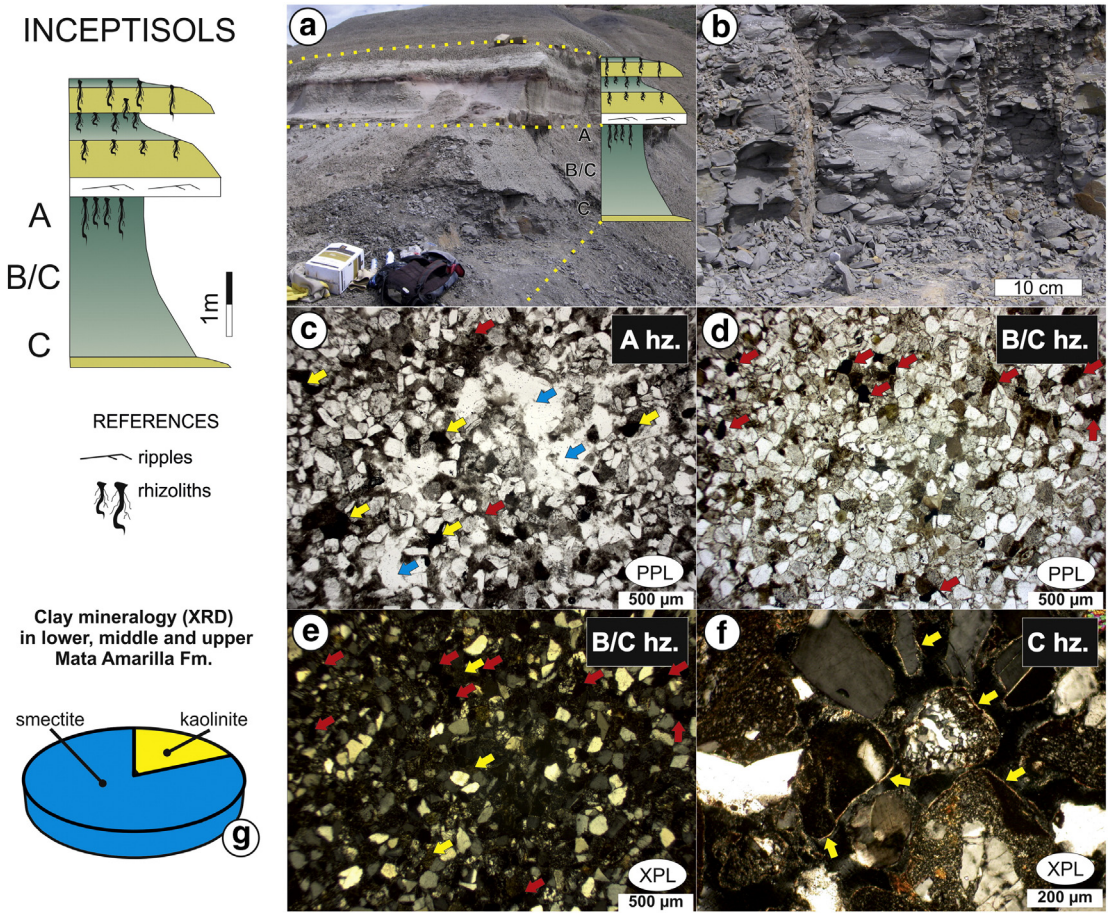

Fig. 4. Inceptisol features. (a) Field picture showing a Inceptisol succession overlying by proximal crevasse splays deposits (yellow arrows), backpack for scale is 80 cm. (b) Detail of gley colored non- to poorly-structured B/C horizon. Detailed micromorphology of (c) A horizon showing gefuric to chitonic c/f related distribution, light to dark brown groundmass (red arrows), chambers and voids (blue arrows), and typic strongly impregnate Fe-Mn nodules with amiboidal morphologies (yellow arrows), PPL. (d) PPL, and (e) XPL, B/C horizon showing light brown with an undifferentiated b-fabric (yellow arrows) and typic strongly impregnate Fe-Mn nodules with amiboidal morphologies (red arrows). (f) C horizon showing medium to coarse sand particles of abundant volcanic lithic grains, quartz and feldspar with a monic c/f related distribution and very thin clay coatings (yellow arrows), XPL. (g) Clay mineralogical composition of Inceptisols from Mata Amarilla Fm. (For interpretation of the references to color in this figure legend, the reader is referred to the web version of this article.)

4.3. Clay-mineralogy of Mata Amarilla Formation paleosols

Clay-fraction XRD analysis of 103 samples shows that smectite is the dominant clay mineral throughout the unit (Supplementary Table 1). It constitutes 92% on average of the clay fraction of all the paleosol types, varying between 32 and 100%. Kaolinite (5% on average, ranging from 0 to 64%), illite (1% on average), chlorite (0.4% on average) and palygorskite (2% on average) are subordinate clay minerals in the analyzed paleosols. On the basis of the presence, type and relative amount of the above-mentioned clay minerals, three clay mineral assemblages have been defined. They are: smectite-dominated assemblage (S), palygorskite-rich assemblage associated with dominant smectite (S-P), and kaolinite-rich assemblage associated with smectite and other clays (S-K). S assemblage (~100% smectite; smectite 96%, kaolinite 3% and illite 1%) is present throughout the Mata Amarilla Formation where Vertisols, the vertic Alfisol and Inceptisols exist. However, some Histosols also have this assemblage (Supplementary Table 1, Fig. 6). The S-P assemblage has on average smectite 55%, palygorskite 38%, kaolinite 4%, chlorite 1%; illite 1% and illite/smectite mixed-layers <1%, and is restricted to the lower section of the Mata Amarilla Formation where Histosols occur (Supplementary Table 1, Fig. 6). The S-K assemblage has on average smectite 44%, kaolinite <43%, illite 7%, chlorite 4% and illite/smectite mixed-layers 1%, and is the least representative clay-mineral assemblage in the Mata Amarilla Formation paleosols. It is only observed in the upper section of the unit in samples of Histosols and Vertisols (Supplementary Table 1, Fig. 6).

A general vertical trend in the arrangement of the clay mineral associations shows a continuous dominance of the S assemblage through the entire succession, which is only interrupted in the lower section by the S-P assemblage, and by the S-K assemblage in the upper section of the Mata Amarilla Formation (Fig. 6).

4.4. Geochemical signature of the paleosols of the Mata Amarilla Formation

Geochemistry of the paleosols shows that the CIA-K weathering index is between 64 and 94 (79.1 on average with a standard deviation of 6.25). The CALMAG weathering index is between 68.3 and 87.5 (81.1 on average with a standard deviation of 3.8). The Al/∑Bases ratio is 1.91 on average with a standard deviation of 0.56. The Al/Si is 0.17 on average with a standard deviation of 0.04. The total iron/alumina (Fe/Al) ratio is 0.16 on average with a standard deviation of 0.004. The Ba/Sr is 1.36 on average with a standard deviation of 0.81. The Ti/Al is 0.04 on average with a standard deviation of 0.01. The K + Na/Al is 0.32 on average with a standard deviation of 0.1 (Supplementary Table 2, Fig. 6).

Although the Mata Amarilla Formation paleosols exhibit stratigraphic variation in most soil molecular ratios, a unit-scale trend in some of them can be observed (Fig. 6). The weathering indices of CIA-K and CALMAG show similar patterns with a strong decrease in the lower part of the middle section of the Mata Amarilla Formation (weathering indices ~ 65; Fig. 6), followed by an upsection increase in weathering index (weathering index ~89). Above, the weathering values are around the background (weathering index ~80) and show another

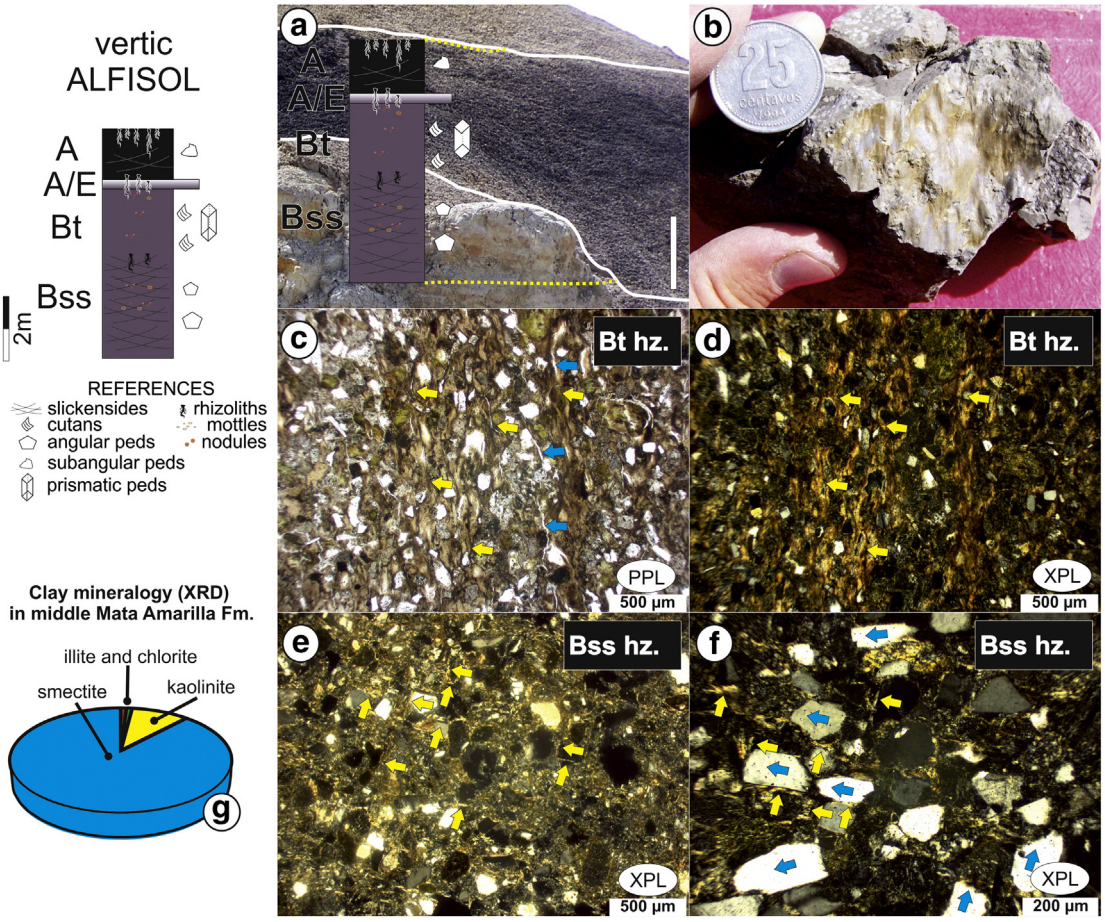

Fig. 5. Vertic Alfisol features. (a) Field picture showing the vertic Alfisol level, bar for scale is 2 m. (b) Detail of dark gray colored prismatic ped showing the brownish clay illuviation surface (cutan) from Bt horizon, coin for scale is 2.2 cm. Detailed micromorphology of (c) PPL, and (d) XPL, Bt horizon showing light to brown groundmass with an undifferentiated b-fabric, and abundant laminated to microlaminated, dense, complete to incomplete dusty illuvial clays infillings (yellow arrows); small vertical voids showing incomplete fillings of rhizolith walls (blue arrows). (e) XPL and (f) XPL, Bss horizon showing light brown to orange color groundmass with cross-striated b-fabric; characterized by two set of birefringent clay orientation ~80° (yellow arrows). (f) Note that b-axes of grains also orientated with the same pattern (blue arrows). (g) Clay mineralogical composition of the vertic Alfisol from Mata Amarilla Fm. (For interpretation of the references to color in this figure legend, the reader is referred to the web version of this article.)

weathering increase in the upper section of the unit (weathering index up to >90). The Al/∑Bases is related to hydrolysis (base loss); the curve shows three abrupt but slight increases (lower and upper parts of the middle section and the lower part of the upper section) and a more constant increase in hydrolysis value to the top of the unit. The Al/Si, related to clayeyness, shows increases in five samples, with a general increase in the lowermost and uppermost part of the middle section of the unit. The Fe/Al, related to oxidation always displays very low values (<0.25); however, there are five increases from background values: near to the lower-middle sections boundary, in the lower, middle and upper parts of the middle section, and in the top of the unit. The Ba/Sr curve, related to leaching, shows variation with a clear increase in the lower part of the middle section. The Ti/Al, related to provenance, does not display any variation. Finally, the K + Na/Al, related to salinization, shows much variation but with a decreasing trend to the top of the unit.

4.5. Paleotemperature and Paleoprecipitation estimates for the Mata Amarilla paleosols

Previous compositional studies in the Mata Amarilla Formation have shown that the primary source of the sandstones was a magmatic arc, and to a much lesser extent, an orogenic area composed of uplifted volcanic and metamorphic rocks; while the fine-grained sediments are characterized by the preponderance of smectite related to the alteration of volcaniclastic materials (Varela et al., 2013). Since the Ti/Al ratio in Mata Amarilla paleosols remains more or less unchanged (μ: 0.04; σ: 0.01) through the entire C° Waring succession, little or no provenance change is indicated through the mid-Cretaceous (Supplementary Table 2, Fig. 6), and a quantitative paleoclimate reconstruction using Al content can be applied to the strata (Fig. 7).

The mid-Cretaceous paleotemperature (MAT) estimates for the Mata Amarilla paleosols using the SAL and PWI proxies show an average of 11.46 °C ± 4.4 °C and 12 °C ± 2.1 °C, respectively (Fig. 7). The MAT calculated using the SAL proxy ranges from 9 ± 4.4 °C to 16 ± 4.4 °C; meanwhile, MAT from the PWI proxy varies between 11 ± 2.1 °C and 14 ± 2.1 °C. Both proxies exhibit a clear increasing upsection trend in MAT. However, a closer inspection shows that both curves display a more or less constant MAT up to the upper section of the formation where an increasing trend up to 16 ± 4.4 °C and 14 ± 2.1 °C, respectively, is observed. At this scale, the SAL-based MAT curve shows two distinct peaks up to 13 ± 4.4 °C, one in the lower part of the middle section (mid-Cenomanian; ~96 Ma), and another in the upper part of the middle section (mid-Turonian; ~91 Ma). The PWI-based MAT curve displays increased values of lower magnitudes.

Paleoprecipitation (MAP) estimates for the Mata Amarilla paleosols using the CALMAG proxy range from 1115 ± 108 to 1557 ± 108 mm/yr with an average of 1404 ± 108 mm/yr. These values are higher than the average MAP calculated from the CIA-K proxy (1059 ± 182 mm yr^{-1}). MAP from CIA-K varied between 787 ± 182 and 1419 ± 182 mm yr^{-1}. MAP estimates from ∑Bases proxy indicate lower values that vary between 827 ± 235 and 1142 ± 235 mm/yr, with an average of

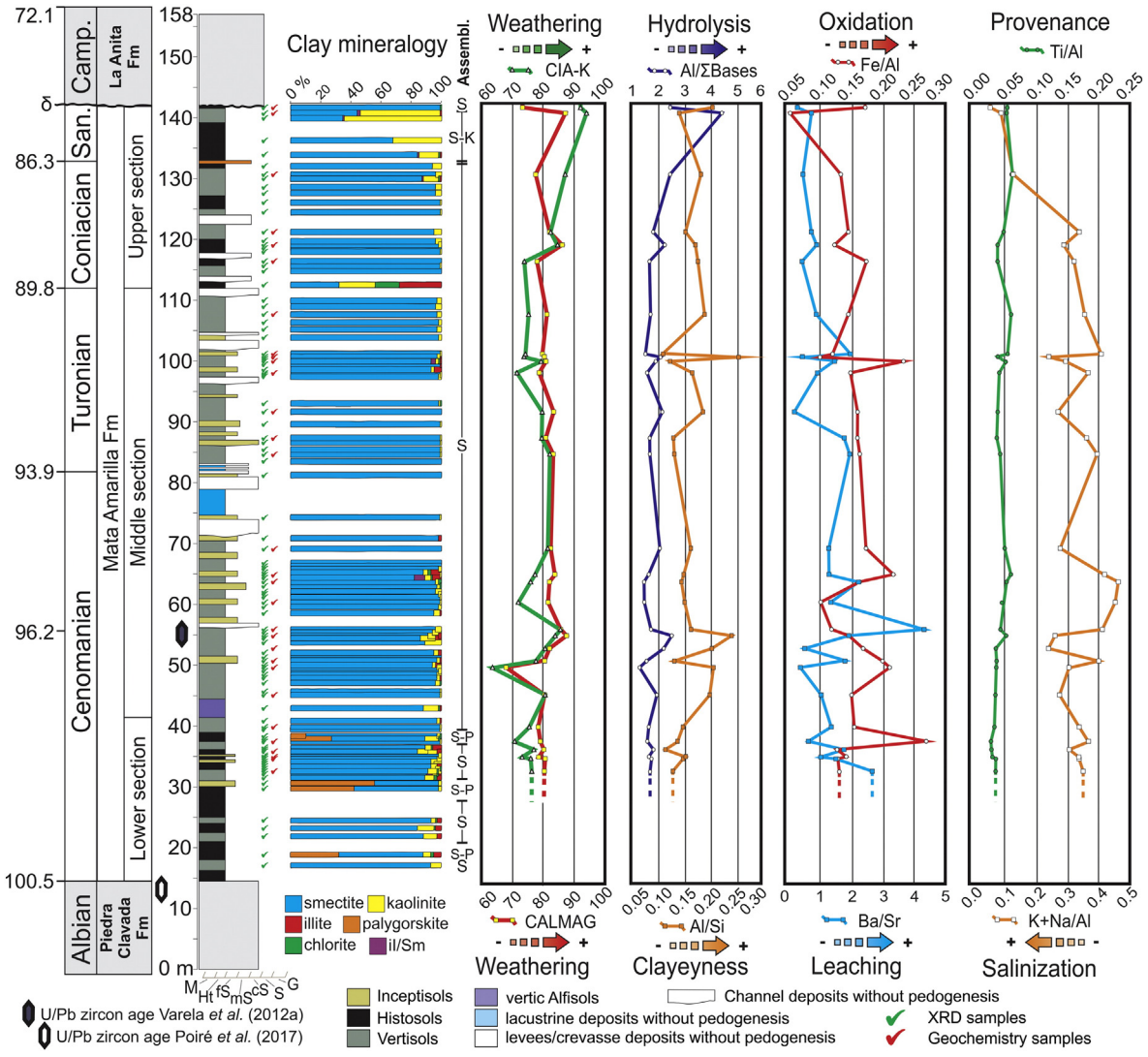

Fig. 6. Clay mineralogy and pedogenic processes indexes based on major element ratios (CIA-K; CALMAG; AL/∑bases; Al/Si; Fet/Al; Ba/Sr; Ti/Al and K + Na/Al) of mid-Cretaceous paleosols of the Mata Amarilla Formation.

919 ± 235 mm/yr. The three estimated MAP curves show similar gross trends. Because the CALMAG proxy provides the most reliable MAP estimates for Vertisols and paleosols with vertic features (Nordt and Dreise, 2010; Adams et al., 2011), MAPs calculated using the CALMAG index are our preferred values (Fig. 7). A common stratigraphic trend is notable between the three proxies, showing slightly higher MAP estimates up section (1549 ± 108 mm/yr). However, a decrease in paleoprecipitation is observable at the lowermost part of the middle section at ~97 Ma (1100 ± 108 mm yr^{-1}), followed by an increase at ~96 Ma (1557 ± 108 mm yr^{-1}). Toward the top of the section there are constant values of MAP (~1404 ± 108 mm yr^{-1}; Fig. 7) up to ~88 Ma, where the MAP values are slightly higher (1525 ± 108 mm/yr).

5. Discussion

5.1. Pedogenic processes

The micromorphological analyses together with the clay mineralogical and geochemical analyses suggest that the main pedogenic processes that occurred in the Mata Amarilla paleosols were: vertization, hydromorphism (gleization), argilluviation or lessivage (clay illuviation), and bioturbation. All of these processes took place under moderate hydrolysis and a wide range of weathering conditions.

The presence of vertic microfeatures such as cross-striated b-fabrics, b-axes of grains oriented with the same pattern, and open porphyric c/f related distribution suggests that vertization constituted one of the main pedogenic processes (Kovda and Mermut, 2010). The clay mineralogy, dominated by smectite (Fig. 6), supports this interpretation. The abundance of smectite is related to the alteration of volcanic glass coming from contemporaneous late Cretaceous ash fall (Patagonian Andean Magmatic Arc source) under a greenhouse climate (Varela et al., 2013).

Hydromorphism related to poor drainage conditions is notable from the presence of Histosols in the lower and upper section of the Mata Amarilla Formation. The presence of Fe-Mn nodules suggests poor drainage conditions (Lindbo et al., 2010), even in the middle section of the Mata Amarilla Formation where Vertisols, Inceptisols and vertic Alfisols are present. Gley colors and low Fe/Al values (<0.25) record the intensity of this process (Fig. 6). Abundant pedogenic smectite in these paleosols also attests to weakly drained or waterlogged conditions in warm seasonal climate conditions with alternating wet and dry seasons (e.g., Thiry, 2000). As mentioned previously, there are five punctuated increases in Fe/Al above background values, which are coincident with the presence of Inceptisols (Fig. 6) developed in areas of the fluvial system with relativelygreater topographic relief where drainage conditions were slightly higher (e.g., levees and crevasse deposits; Varela et al., 2012b) and therefore were subjected to more oxidization.

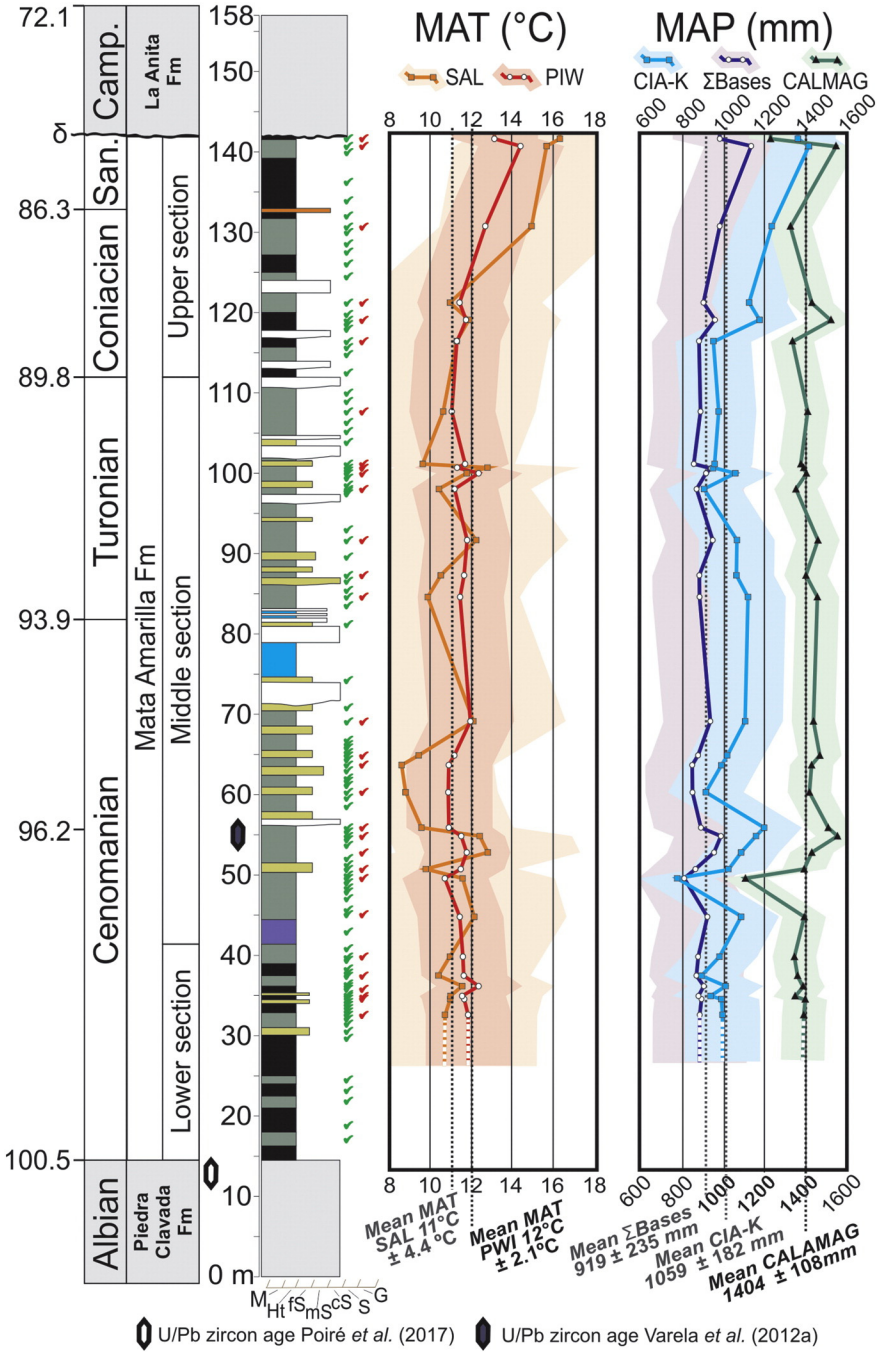

Fig. 7. Mean annual temperature (MAT) and mean annual precipitation (MAP) estimation curves for the Mata Amarilla's paleosols. The shaded areas of each curve correspond to the standard error of each climofunction.

Also, the clay composition of the Inceptisols shows an increase in pedogenic kaolinite content related to rapid circulation of interstitial waters and chemical weathering of a more porous parent material (e.g., Raigemborn et al., 2014).

The presence of thick laminated to microlaminated dusty clay coatings covering rhizolith walls, and dense complete to incomplete clay infillings in Bt/Btss horizons, both from Alfisols and Vertisols, provides evidence for clay illuviation (Kühn et al., 2010) (Figs. 2, 5). These pedofeatures together with the predominance of pedogenic smectite point to seasonality in water availability. An extended dry season is inferred due to the presence of well-defined banding of the clay coatings (e.g., Retallack et al., 2000). Clay enrichment or clayeyness can be inferred from Al/Si. The high levels of Al/Si (μ: 0.16; Fig. 6) suggest clay enrichment in B horizons by illuviation. The positive peaks in the Al/Si curve are coincident with the presence of argillic Bt horizons both in vertic Alfisols and Vertisols (Fig. 6).

Bioturbation is recorded by the occurrence of abundant rhizoliths (Fig. 2c), voids, chambers and channels (Fig. 2c–d, 3c–f, 4c) in thin sections. The presence of chambers and channels represent the modification of the groundmass by earthworms (e.g. Stolt and Lindbo, 2010; Kooistra and Pulleman, 2010; Kooistra, 2015). The high content of fossil leaves, trunks, organic remains and big Mn-nodules associated with stumps in the Mata Amarilla paleosols (Iglesias et al., 2007; Varela et al., 2016; Martinez et al., 2017), and the thickness (~2 m) of the Bt/Btss horizons, suggest a high biomass of plant and invertebrate soil fauna (Retallack, 2001).

The weathering CIA-K index is near the mild-strong weathering limit (μ: 79.1; Sheldon and Tabor, 2009), whereas the CALMAG weathering

index is slightly over it (μ: 81.1). The relatively high Ba/Sr (1.36 on average) indicates leaching that peaked at ~96 Ma (Fig. 6). The Al/∑Bases (hydrolysis) curve is ~2 on average suggesting a moderate loss of exchangeable bases. This curve presents three slight increases (mid-Cenomanian; mid-Turonian and lower Coniacian). A more constant increasing trend in hydrolysis values to the top of the unit is observed. This trend is coincident with an increase of both weathering indices (CIA-K and CALMAG) and kaolinite content (Fig. 6), suggesting that the increase in precipitation and temperature favored weathering (Fig. 7).

The rare presence of palygorskite in the Histosols of the lower section of the Mata Amarilla Formation was interpreted as related to coastal environments where paleosols developed under poorly drained conditions (Varela et al., 2013). In such paralic environments the high Si and Mg content of groundwater, related to the sporadic incursion of brackish waters (Varela et al., 2011; Griffin and Varela, 2012), favored the formation of palygorskite at the expense of other silicate precursors, probably smectite, which provided the necessary Al for its formation (Pimentel, 2002; Arribas et al., 2004). These, results are comparable to the similar preservation of coarse organic fragments in Mata Amarilla Histosols and in modern Histosols of a tidal marsh (Stolt and Lindbo, 2010).

5.2. Paleoclimatic reconstruction

PWI paleotemperatures calculated from the mid-Cretaceous Mata Amarilla Formation range from 11 to 14 ± 2.1 °C, with an average of 12 ± 2.1 °C. The paleoprecipitation estimates using the more accurate proxy for Vertisols (CALMAG; Nordt and Dreise, 2010) range from 1115 ± 108 to 1557 ± 108 mm yr, with an average of 1404 ± 108 mm yr (Fig. 7). Such values are similar to modern temperate humid subtropical climate, following the climate classification of Zhang et al. (2016).

The combination of data derived from the Mata Amarilla paleosols demonstrates that at ~60° south paleolatitude of mid-Cretaceous South America, the climate was temperate–warm and humid with marked seasonality. These new data confirm climate estimates previously interpreted from angiosperm fossil floras described by Iglesias

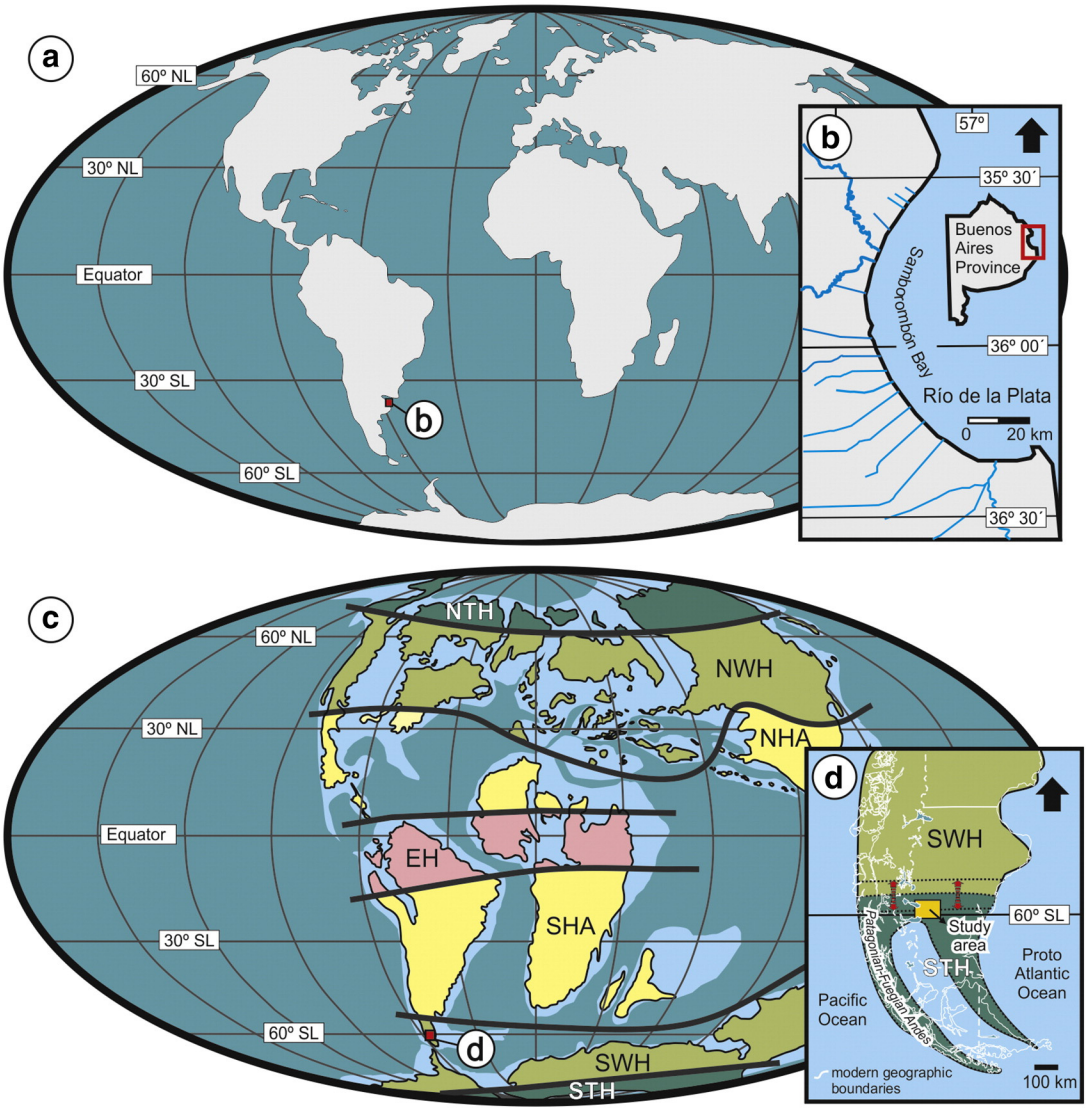

Fig. 8. (a) Actual global paleogeographic map. (b) Detail of Samborombón bay wetland area. (c) Mid-Cretaceous global paleogeographic reconstruction from Scotese (1991) and global paleoclimatic reconstruction from Chumakov (1995) modified by Spicer and Skelton (2003). NTH: Northern High-latitude Temperate humid belt, STH: Southern High-latitude Temperate humid belt, NWH: Northern Mid-latitude Warm humid belt, SWH: Southern Mid-latitude Warm humid belt, NHA: Northern Hot Arid belt, EH: Equatorial Humid belt, SHA: Southern Hot Arid belt. (d) Detail of the study area showing the paleogeographic position during mid-Cretaceous time, according to Van Hinsbergen et al. (2015) and the modificated position of SWH and STH belts. Red arrows indicate the variation from the average MAT data. (For interpretation of the references to color in this figure legend, the reader is referred to the web version of this article.)

et al. (2007) and analysis of fossil gymnosperms logs and Cycadales (Varela et al., 2016; Martinez et al., 2017), as well as the presence of Perforissidae, Cupedidae and related plant-insect interactions in the Mata Amarilla Formation (Petrulevičius et al., 2014). Iglesias et al. (2011) interpreted the flora of southern Patagonia (Mata Amarilla Formation) as indicative of a high temperature and rainfall/humidity climate, and situated in a Warm Temperate Biome (Iglesias et al., 2007, 2011).

Modern day analogs for the Mata Amarilla Formation paleosols can be found in wetlands of Samborombón Bay (Buenos Aires Province, Argentina, 36° S; Fig. 8a). At this site, similar pedogenic processes have developed Vertisols and less abundant vertic Mollisols, according to the soil maps of the region (Imbellone et al., 2000, 2009, 2010; INTA, 2015). This modern wetland resembles those of the Mata Amarilla wetlands in that they both formed under temperate humid subtropical climate conditions (e.g., Zhang et al., 2016). Samborombón Bay has MAT values of 14 °C and MAP values close to 1000 mm yr, with seasonality in rainfall distribution (Carol et al., 2013; INTA, 2015; Carol and Alvarez, 2016). Although the sedimentary environments and the related soils of Samborombón Bay (36°S) are nearly identical to those interpreted for the Mata Amarilla Formation (~60°S; Fig. 8b), rainfall conditions are lower in Samborombón Bay (−400 mm yr) and temperatures are slightly higher. Modern day southern Argentina (Patagonia), where the Mata Amarilla Formation outcrops (50° south latitude), has a dry cold desert climate following Zhang et al. (2016) (Fig. 8a). The presence of paleosols corresponding to temperate humid subtropical climates at ~60°S would indicate that, during the mid-Cretaceous greenhouse, subtropical areas were displaced towards the poles by ~25° paleolatitude in South America.

5.3. Paleoclimatic implications of southern Patagonia paleosols in mid-Cretaceous global climate reconstructions

Global climate models for the mid-Cretaceous suggest high atmospheric pCO_2 levels that gave rise to warm surface temperatures. The moderate increase in temperatures resulting from greenhouse gases were amplified by feedback mechanisms including decreases in albedo and thermal insulation due to the melting of polar ice caps (Barron, 1983; Barron et al., 1989; Caldeira and Rampino, 1991; Frakes, 1999; Poulsen et al., 1999, 2001, 2007; Floegel and Wagner, 2006; Royer, 2010; Hay, 2011). These models suggest that in high mid-latitudes in the Northern Hemisphere, paleotemperatures increased by 35 °C during the winter and only 7.5 °C during the summer, thereby decreasing the temperature gradient during both seasons (i.e., less marked seasonality). Further, mid-Cretaceous rainfall estimates based on $\delta^{18}O$ data from paleosol sphaerosiderites along the Cretaceous Western Interior Seaway (between 54° to 28° north paleolatitude) ranged from 2500 to 4100 mm/yr (White et al., 2001) and from 2600 to 3300 mm/yr (Ufnar et al., 2002, 2004). The data from the Mata Amarilla Formation support the models by providing data for benchmarking – the climofunction estimates presented here agree with model results (i.e., rainfall and temperatures increases at mid-to high latitudes) - however, they show slightly lower values of MAT and MAP and a more marked seasonality than those recorded from the same latitudes in the Northern Hemisphere. At high latitudes, the mean annual temperatures deduced from plant fossil assemblages reached 9 °C during the mid-Cretaceous in northern Siberia (Herman and Spicer, 1996) and 10 °C in northern Alaska and the Antarctic Peninsula (Spicer and Corfield, 1992; Spicer et al., 1993; Spicer and Herman, 2001). In addition, Fletcher et al. (2014) estimated MAT of 13.6 ± 2 °C and MAP of 1646 ± 379 mm/yr based on CLAMP analysis of flora from the mid-Cretaceous Winton Formation of central-western Queensland, Australia. The Mata Amarilla angiosperms and gymnospern floras, and Cycadales and gymnosperm ring analysis, also suggest high temperature and rainfall/humidity with marked seasonality (Iglesias et al., 2007, 2011; Varela et al., 2016; Martinez et al., 2017). The global paleoclimate reconstruction from Chumakov (1995) modified by Spicer and Skelton (2003) suggest that the study area was in the mid-Cretaceous Southern Warm Humid belt (SWH; Fig. 8c). However, our data suggest that the study area probably was near the limit between Southern Temperate and Warm Humid belts (STH and SWH; Fig. 8d). Towards the mid latitude areas corresponding to the Southern Hot Arid belt (STH; Fig. 8d), dry paleoclimate conditions have been recorded in paleosols from different proxies (macro- and micromorphologically, geochemically and paleoecologically), both in the Northwestern Argentina and Southeastern Brazil (Basilici et al., 2009, 2016, 2017; Dal' Bó et al., 2010). In the future, more terrestrial paleoclimatic work should focus on mid-to high latitudes in the Southern Hemisphere to polish the current mid-Cretaceous reconstruction.

6. Conclusions

The main pedogenic processes recognized in the Mata Amarilla Formation paleosols are vertization, hydromorphism (gleization), argilluviation (clay illuviation) and bioturbation. These processes occurred under elevated chemical weathering rates resulting in moderate losses of exchangeable bases typical of temperate–warm and humid climates with marked seasonality, all acting on fine volcaniclastic parent material in a wetland environment. The preponderance of smectite is related to the alteration of volcaniclastic materials, the increment of kaolinite content is related to the increase of weathering and hydrolysis towards the top of the unit, and the presence of palygorskite is related to coastal environmental conditions. The paleotemperature of the mid-Cretaceous Mata Amarilla Formation calculated by PWI shows MATs ranging from 11 to 14 ± 2.1 °C, with an average of 12 ± 2.1 °C. The paleoprecipitation estimates using the more accurate proxy for Vertisols (CALMAG) indicates that MAPs ranged from 1115 ± 108 to 1557 ± 108 mm/yr, with an average of 1404 ± 108 mm/yr. These MAT and MAP values suggest that at ~60° south paleolatitude during the mid-Cretaceous greenhouse episode, a temperate humid subtropical climate occurred. Currently, similar conditions exist at mid-latitudes in Argentina (~36°S) suggesting that mid-Cretaceous subtropical conditions were displaced by ~25° towards the poles in South America. The results of this work show a more marked seasonality and slightly lower values of MAT and MAP than predictions from global climate models.

Supplementary data to this article can be found online at https://doi.org/10.1016/j.sedgeo.2017.11.001.

Acknowledgments

The authors deeply thanks to the Editor J. Knight, G. Basilici and two anonymous referees for their comments and corrections on the first version of this manuscript. This research was funded by the Agencia Nacional de Promoción Científica y Tecnológica (PICT 2012-0828 awarded to A.N. Varela) and Subsidio Jóvenes Investigadores de la UNLP 2013 (La Plata University Exp. Cod.100 N°19333/2/13 awarded to A.N. Varela). The authors would like to thank P. García, A. Iglesias for their assistance in the field and to A. Poggi, D. Mártire, P. García and C. Genazzini for sample preparation.

References

Adams, J.S., Kraus, M.J., Wing, S.L., 2011. Evaluating the use of weathering indices for determining mean annual precipitation in the ancient stratigraphic record. Palaeogeography, Palaeoclimatology, Palaeoecology 309, 358–366.

Archangelsky, S., 2009. Biogeographic implications of Albian Mohria-like spores (family Anemiaceae) in SW Gondwana (Patagonia). Review of Palaeobotany and Palynology 157, 301–308.

Arribas, M.E., Bustillo, A., Tsige, M., 2004. Lacustrine chalky carbonates: origin, physical properties and diagenesis (Palaeogene of the Madrid Basin, Spain). Sedimentary Geology 166, 335–351.

Barron, E.J., 1983. A warm equable Cretaceous: the nature of the problem. Earth-Science Reviews 19, 305–338.

Barron, E.J., Hay, W.W., Thompson, S., 1989. The hydrologic cycle. A major variable during Earth history. Palaeogeography, Palaeoclimatology, Palaeoecology 75, 157–174.

Basilici, G., Dal' Bó, P.F.F., Ladeira, F.S.B., 2009. Climate-induced sediment-palaeosol cycles in a Late Cretaceous dry aeolian sand sheet: Marília Formation (north-west Bauru Basin, Brazil). Sedimentology 56, 1876–1904.

Basilici, G., Dal' Bó, P.F.F., Ferreira de Olivera, E., 2016. Distribution of palaeosols and deposits in the temporal evolution of a semiarid fluvial distributary system (Bauru Group, Upper Cretaceous, SE Brazil). Sedimentary Geology 341, 245–264.

Basilici, G., Hechenleitner, E.M., Fiorelli, L.E., Dal' Bó, P.F.F., Mountney, N.P., 2017. Preservation of titanosaur egg clutches in Upper Cretaceous cumulative palaeosols (Los Llanos Formation, La Rioja, Argentina). Palaeogeography, Palaeoclimatology, Palaeoecology 482, 83–102.

Biscaye, P.E., 1965. Mineralogy and sedimentation of recent deep sea clay in the Atlantic Ocean and adjacent seas and oceans. Geological Society of America Bulletin 76, 803–832.

Bowman, V., 2015. Antartic palynological and palaeoclimate - a review. Bionature 35, 1–6.

Bullock, P., Federoff, N., Jongerius, A., Stoops, G., Tursina, T., 1985. Handbook for Soil Thin Section Description. Waine Research Publications, Albrighton 152 pp.

Caldeira, K., Rampino, M.R., 1991. The mid-Cretaceous superplume, carbon dioxide, and global warming. Geophysical Research Letters 18, 987–990.

Cantrill, D.J., Poole, I., 2012. The Vegetation of Antarctica Through Geological Time. Cambridge University Press, Cambridge 480 pp.

Carol, E., Alvarez, M.P., 2016. Processes regulating groundwater chloride content in marshes under different environmental conditions: a comparative case study in Península Valdés and Samborombón Bay, Argentina. Continental Shelf Research 115, 33–43.

Carol, E., Kruse, E., Tejada, M., 2013. Surface water and groundwater response to the tide in coastal wetlands: assessment of a marsh in the outer Río de la Plata estuary, Argentina. Journal of Coastal Research 65, 1098–1103.

Chumakov, N.M., 1995. Climatic zones in the middle of the Cretaceous Period. Stratigraphy and Geological Correlation 3, 3–14.

Dal' Bó, P.F.F., Basilici, G., Angélica, R.S., 2010. Factors of paleosol formation in a Late Cretaceous eolian sand sheet paleoenvironment, Marília Formation, Southeastern Brazil. Palaeogeography, Palaeoclimatology, Palaeoecology 292, 349–365.

Fletcher, T.L., Greenwood, D.R., Moss, P.T., Salisbury, S.W., 2014. Paleoclimate of the Late Cretaceous (Cenomanian-Turonian) portion of the Winton Formation, Central-Western Queensland, Australia: new observation based on CLAMP and bioclimatic analysis. PALAIOS 29, 121–128.

Floegel, S., Wagner, T., 2006. Insolation-control on the Late Cretaceous hydrological cycle and tropical African climate-global climate modeling linked to marine climate records. Palaeogeography, Palaeoclimatology, Palaeoecology 235, 288–304.

Frakes, L.A., 1999. Estimating the global thermal state from Cretaceous sea surface and continental temperature data. In: Barrera, E., Johnson, C. (Eds.), Evolution of the Cretaceous Oceanic Climate System. Geological Society of America Special Paper vol. 332, pp. 49–57.

Gallagher, T.M., Sheldon, N.D., 2013. A new paleothermometer for forest palaeosols and its implications for Cenozoic climate. Geology 41, 647–650.

Griffin, M., Varela, A.N., 2012. Systematic palaeontology and taphonomic significance of the mollusc fauna from the Mata Amarilla Formation (lower Upper Cretaceous), Southern Patagonia, Argentina. Cretaceous Research 37, 164–176.

Hay, W.W., 2011. Can humans force a return to a 'Cretaceous' climate? Sedimentary Geology 235, 5–26.

Herman, A.B., Spicer, R.A., 1996. Paleobotanical evidence for a warm Cretaceous Arctic Ocean. Nature 380, 330–333.

Hyland, E.G., Sheldon, N.D., 2016. Examining the spatial consistency of palaeosol proxies: Implications for palaeoclimatic and palaeoenvironmental reconstructions in terrestrial sedimentary basins. Sedimentology 63, 959–971.

Hyland, E.G., Sheldon, N.D., Van der Voo, R., Badgley, C., Abrajevitch, A., 2015. A new paleoprecipitation proxy based on soil magnetic properties: implications for expanding paleoclimate reconstructions. Geological Society of America Bulletin 127, 975–981.

Iglesias, A., Zamuner, A.B., Poiré, D.G., Larriestra, F., 2007. Diversity, taphonomy, and palaeoecology of an angiosperm flora from the Cretaceous (Cenomanian-Coniacian) in Southern Patagonia, Argentina. Palaeontology 50, 445–466.

Iglesias, A., Artabe, A.E., Morel, E.M., 2011. The evolution of Patagonian climate and vegetation from the Mesozoic to the present. Biological Journal of the Linnean Society 103, 409–422.

Imbellone, P.A., Guichon, B.A., Giménez, J.E., 2000. Eh, Fe^{+2} and Mn^{+2} in wetland soils of La Plata River coastal plain, Argentina. 17th International Congress of Soils Science. Bangkok, Thailand, Symposium 613, pp. 1–10.

Imbellone, P.A., Guichon, B.A., Giménez, J.E., 2009. Hydromorphic soils of Río de La Plata coastal plain, Argentina. Latin America Journal of Sedimentology and Basin Analysis 16, 3–18.

Imbellone, P.A., Giménez, J.E., Panigatti, J.L., 2010. Suelos de la Región Pampeana: Procesos de formación. Ediciones INTA, Buenos Aires 320 pp.

INTA, 2015. Carta de suelos de la provincia de Buenos Aires. Instituto de Suelos http://inta.gob.ar/documentos/carta-de-suelos-de-la-provincia-de-buenos-aires.

Kooistra, M., 2015. Descripción de los componentes orgánicos del suelo. In: Loaiza, J.C., Stoops, G., Poch, R., Casamitjana, M. (Eds.), Manual de micromorfología de suelos y técnicas complementarias. Fondo Editorial Pascual Bravo, Medellin, Colombia, pp. 261–292.

Kooistra, M.J., Pulleman, M.M., 2010. Features related to faunal activity. In: Stoops, G., Marcelino, V., Mees, F. (Eds.), Interpretation of Micromorphological Features of Soils and Regoliths. Elsevier, Amsterdam, pp. 397–418.

Kovda, I., Mermut, A., 2010. Vertic features. In: Stoops, G., Marcelino, V., Mees, F. (Eds.), Interpretation of Micromorphological Features of Soils and Regoliths. Elsevier, Amsterdam, pp. 109–127.

Kühn, P., Aguilar, J., Miedema, R., 2010. Textural features and related horizons. In: Stoops, G., Marcelino, V., Mees, F. (Eds.), Interpretation of Micromorphological Features of Soils and Regoliths. Elsevier, Amsterdam, pp. 217–250.

Lal, R., 1999. Soil management and restoration for C sequestration to mitigate the accelerated greenhouse effect. Progress in Environmental Science 1, 307–326.

Lal, R., 2004. Soil carbon sequestration to mitigate climate change. Geoderma 123, 1–22.

Lindbo, D.L., Stolt, M.H., Vepraskas, M.J., 2010. Redoximorphic features. In: Stoops, G., Marcelino, V., Mees, F. (Eds.), Interpretations of Micromorphological Features of Soils and Regoliths. Elsevier, Amsterdam, pp. 129–147.

Ludvigson, G.A., Joeckel, R.M., Murphy, L.R., Stockli, D.F., González, L.A., Suarez, C.A., Kirkland, J.I., Al-Suwaidi, A., 2015. The emerging terrestrial record of Aptian-Albian global change. Cretaceous Research 56, 1–24.

Martinez, L.C.A., Iglesias, A., Artabe, A.E., Varela, A.N., Apesteguía, S., 2017. A new *Encephalarteas* trunk (Cycadales) from the Cretaceous of Patagonia (Mata Amarilla Formation, Austral basin), Argentina. Cretaceous Research 72, 81–94.

Maynard, J.B., 1992. Chemistry of modern soils as guide for interpreting Precambrian palaeosols. The Journal of Geology 100, 279–289.

Moore, D.M., Reynolds Jr., R.C., 1989. X-ray Diffraction and the Identification and Analysis of Clay Minerals. Oxford University Press, Oxford 329 pp.

Nordt, L.C., Dreise, S.D., 2010. New weathering index improves paleorainfall estimates from vertisols. Geology 38, 407–410.

Parrish, J.T., Daniel, I.L., Kennedy, E.M., Spicer, R.A., 1998. Paleoclimatic significance of mid-Cretaceous flora from Middle Clarence Valley, New Zealand. PALAIOS 13, 149–159.

Petrulevičius, J., Varela, A.N., Iglesias, A., Zamuner, A.B., Poiré, D.G., 2014. First Cenomanian record of insects in the Southern Hemisphere, with Perforissidae (Fulgoroidea) and Cupedidae (Coleoptera) from Southern Patagonia, Argentina. Cretaceous Research 51, 174–185.

Pimentel, N.L.V., 2002. Pedogenic and early diagenetic processes in Palaeogene alluvial fan and lacustrine deposits from the Sado Basin (S Portugal). Sedimentary Geology 148, 123–138.

Poiré, D.G., Iglesias, A., Varela, A.N., Richiano, S., Ibañez Mejías, M., Strömberg, C.A.E., 2017. Edades U-Pb en zircones de tobas de la Fm. Piedra Clavada, Pcia. de Santa Cruz, Argentina: Un marcador Albiano tardío para la evolución tectónica y biológica de la Cuenca Austral. Actas del XX Congreso Geológico Argentino, San Miguel de Tucumán, pp. 95–98.

Pole, M., Philippe, M., 2010. Cretaceous plant fossils of Pitt Island, the Chatham group, New Zealand. Alcheringa 34, 231–263.

Poulsen, C.J., Barron, E.J., Johnson, C., Fawcett, P., 1999. Links between major climatic factors and regional oceanic circulation in the mid-Cretaceous. In: Barrera, E., Johnson, C. (Eds.), Evolution of the Cretaceous oceanic climate system. Geological Society of America Special Paper vol. 332, pp. 73–90.

Poulsen, C.J., Barron, E.J., Arthur, M.A., Peterson, W.H., 2001. Response of the mid-Cretaceous global Oceanic circulation to tectonic and CO_2 forcings. Paleoceanography 16, 576–592.

Poulsen, C.J., Pollard, D., White, T.S., 2007. General circulation model simulation of the δ^{18}Ocontent of continental precipitation in the middle Cretaceous: a model-proxy comparison. Geology 35, 199–202.

Raigemborn, M.S., Gómez-Peral, L., Krause, J.M., Matheos, S.D., 2014. Controls on clay mineral assemblages in an Early Paleogene nonmarine succession: implications for the volcanic and paleoclimatic record of extra-Andean Patagonia, Argentina. Journal of South American Earth Sciences 52, 1–23.

Retallack, G.J., 1993. Classification of palaeosols: discussion and reply. Discussion. Geological Society of America Bulletin 105, 1635–1637.

Retallack, G.J., 2001. Soils of the Past: An Introduction to Paleopedology. Blackwell Science Ltd., Oxford 404 pp.

Retallack, G., Bestland, E., Fremd, T. (Eds.), 2000. Eocene and Oligocene paleosols of Central Oregon. Geological Society of America, Special Paper 344, 1–192.

Royer, D.L., 2010. Fossil soils constrain ancient climate sensitivity. Proceedings of the National Academy of Sciences of the United States of America 107, 517–518.

Scotese, C.R., 1991. Jurassic and cretaceous plate tectonic reconstructions. Palaeogeography, Palaeoclimatology, Palaeoecology 87, 493–501.

Sheldon, N.D., 2006. Abrupt chemical weathering increase across the Permian-Triassic boundary. Palaeogeography, Palaeoclimatology, Palaeoecology 231, 315–321.

Sheldon, N.D., Tabor, N.J., 2009. Quantitative paleoenvironmental and paleoclimate reconstruction using palaeosols. Earth Science Reviews 85, 1–52.

Sheldon, N.D., Retallack, G., Tanaka, S., 2002. Geochemmical climofunctions from North American soils and application to palaeosols across the Eocene Oligocene boundary in Oregon. Journal of Geology 110, 687–696.

Soil Survey Staff, 1975. Soil Taxonomy. United States Department of Agriculture, Washington, DC.

Soil Survey Staff, 1998. Key to Soil Taxonomy. 8th edn. United States Department of Agriculture, Natural Resources Conservation Service, Washington, DC.

Spicer, R.A., Corfield, R.M., 1992. A review of terrestrial and marine climates in the Cretaceous with implications for modelling the 'greenhouse Earth'. Geological Magazine 129, 169–180.

Spicer, R.A., Herman, A.B., 2001. The Albian-Cenomanian flora of the Kukpowruk River, western North Slope, Alaska: stratigraphy, palaeofloristics, and plant communities. Cretaceous Research 22, 1–40.

Spicer, B., Skelton, P.W., 2003. The operation of the major geological carbon sinks. In: Skelton, P. (Ed.), The Cretaceous World. Cambridge University Press, Cambridge, United Kingdom, pp. 249–272.

Spicer, R.A., Rees, P.M., Chapman, J.L., Jarzembowski, E.A., Cantrill, D., 1993. Cretaceous phytogeography and climate signals [and discussion]. Philosophical Transactions of the Royal Society of London B 341, 277–286.

Stolt, M.H., Lindbo, D.L., 2010. Soil organic matter. In: Stoops, G., Marcelino, V., Mees, F. (Eds.), Interpretation of Micromorphological Features of Soils and Regoliths. Elsevier, Amsterdam, pp. 369–396.
Stoops, G., 2003. Guidelines for Analysis and Descriptions of Soil and Regolith Thin Sections. Soil Science Society of America, Madinson, Wisconsin 184 pp.
Thiry, M., 2000. Palaeoclimatic interpretation of clay minerals in marine deposits: an outlook from the continental origin. Earth-Science Reviews 49, 201–221.
Ufnar, D.F., González, L.A., Ludvigson, G.A., Brenner, R.L., Witzke, B.J., 2002. The mid-cretaceous water bearer: isotope mass balance quantification of the Albian hydrologic cycle. Palaeogeography, Palaeoclimatology, Palaeoecology 188, 51–71.
Ufnar, D.F., Ludvigson, G.A., González, L.A., Brenner, R.L., Witzke, B.J., 2004. High latitude meteoric $\delta^{18}O$ composition: Paleosol siderite in the mid-Cretaceous Nanushuk Formation, North Slope, Alaska. Geological Society of America Bulletin 116, 463–473.
Van Hinsbergen, D.J.J., de Groot, L.V., van Schaik, S.J., Spakman, W., Bijl, P.K., Sluijs, A., Langereis, C.G., Brinkhuis, H., 2015. A paleolatitude calculator for palaeoclimate studies. PLoS One 10, e0126946. https://doi.org/10.1371/journal.pone.0126946.
Varela, A.N., 2015. Tectonic control of accommodation space and sediment supply within the Mata Amarilla Formation (lower Upper Cretaceous) Patagonia, Argentina. Sedimentology 62, 867–869.
Varela, A.N., Richiano, S., Poiré, D.G., 2011. Tsunami vs storm origin for shell bed deposits in a lagoon environment: an example from the Upper Cretaceous of Southern Patagonia, Argentina. Latin America Journal of Sedimentology and Basin Analysis 18, 63–85.
Varela, A.N., Poiré, D.G., Martin, T., Gerdes, A., Goin, F.J., Gelfo, J.N., Hoffmann, S., 2012a. U-Pb zircon constraints on the age of the Cretaceous Mata Amarilla Formation, Southern Patagonia, Argentina: its relationship with the evolution of the Austral Basin. Andean Geology 39, 359–379.
Varela, A.N., Veiga, G.D., Poiré, D.G., 2012b. Sequence stratigraphic analysis of Cenomanian greenhouse palaeosols: a case study from southern Patagonia, Argentina. Sedimentary Geology 271 (272), 67–82.
Varela, A.N., Gómez-Peral, L.E., Richiano, S., Poiré, D.G., 2013. Distinguishing similar volcanic source areas from an integrated provenance analysis: implications for foreland Andean basins. Journal of Sedimentary Research 83, 258–276.
Varela, A.N., Iglesias, A., Poiré, D.G., Zamuner, A.B., Richiano, S., Brea, M., 2016. Petrified forests in the Austral Basin marks a Cenomanian forced regression heterogeneous surface. Geobiology 14, 293–313.
White, T., González, L., Ludvigson, G., Poulsen, C., 2001. Middle Cretaceous greenhouse hydrologic cycle of North America. Geology 29, 363–366.
White, T., Witzke, B., Ludvigson, G., Brenner, R., 2005. Distinguishing base-level change and climate signals in a Cretaceous alluvial sequence. Geology 33, 13–16.
Zhang, L., Wang, C., Li, X., Cao, K., Song, Y., Hu, B., Lu, D., Wang, Q., Du, X., Cao, S., 2016. A new paleoclimate classification for deep time. Palaeogeography, Palaeoclimatology, Palaeoecology 443, 98–106.